Available online at www.sciencedirect.com
SCIENCE DIRECT®
International Journal of Heat and Fluid Flow 26 (2005) 233–243
International Journal of HEAT AND FLUID FLOW
www.elsevier.com/locate/ijhff

Experimental and numerical study of turbulent heat transfer on a cylindrical pedestal

Bart Merci [a,*], Masood P.E. Mesbah [b], James W. Baughn [c]

[a] Ghent University, Department of Flow, Heat and Combustion Mechanics, Sint Pietersnieuwstraat 41 B-9000 Gent, Belgium
[b] Department of Water Resources, State of California, Sacramento, USA
[c] Department of Mechanical and Aeronautical Engineering, University of California, Davis, USA

Received 3 October 2003; accepted 2 September 2004
Available online 5 November 2004

Abstract

Experimental data are presented of local surface heat transfer coefficients in a turbulent axisymmetric jet, impinging onto a cylindrical pedestal, mounted on a flat plate. The preheated wall transient method is applied with liquid crystals. Simulation results with standard two-equation turbulence models reveal strong deviations from the experimental data. Therefore, a two-equation turbulence model is used, incorporating effects from streamline curvature in the eddy viscosity and reducing turbulence production in stagnation flow regions through the dissipation rate transport equation and the turbulent viscosity. It is illustrated that this leads to accurate heat transfer predictions. For the turbulent heat transfer, the linear gradient diffusion hypothesis is applied. Heat transfer is examined on the pedestal top and side face, as well as on the plate. Different Reynolds numbers and nozzle–pedestal distances are considered.

Keywords: Convective turbulent heat transfer; Pedestal on flat plate; Experimental data; Simulation results; Turbulence model

1. Introduction

Increasing local heat transfer is of importance in many technical applications. To that purpose, impinging jets are widely used due to their high convective heat transfer rates. Many experimental studies have been performed on a flat plate (Baughn and Shimizu, 1989; Baughn et al., 1991; Lytle and Webb, 1994; Yan, 1993). In the current paper, experimental data are presented for local turbulent convective heat transfer on a cylindrical pedestal, mounted on a flat plate.

In machinery design, numerical simulations play an increasingly important role. Local heat transfer predictions in turbulent impinging jets are, however, inaccurate with standard turbulence models (Behnia et al., 1999; Craft et al., 2000; Merci and Dick, 2003). In Merci and Dick (2003) and Merci et al. (2004), a k–ε model is presented which does yield accurate results for impinging jet heat transfer on a flat plate, without case specific parameter tuning. In the current paper, the first-order model as in Merci et al. (2004) is applied to the more complex case of impingement heat transfer on the cylindrical pedestal, mounted on a flat plate.

The most extensive set of comparisons of the simulation results to the experimental data, is presented for a Reynolds number $Re = 23{,}000$, based on the mean jet velocity and the nozzle diameter. The distance between the nozzle exit and the pedestal top face is equal to six nozzle diameters. The influence of variations in the Reynolds number and variations of nozzle–pedestal distance is examined on the stagnation point heat transfer coefficient. It is illustrated that standard two-equation turbulence models (i.e. the standard k–ε model by Jones

* Corresponding author. Tel.: +32 9 264 33 14; fax: +32 9 264 35 86.
E-mail address: bart.merci@ugent.be (B. Merci).

0142-727X/$ - see front matter © 2004 Elsevier Inc. All rights reserved.
doi:10.1016/j.ijheatfluidflow.2004.09.002

Nomenclature

c_p	specific heat capacity at constant pressure	T	temperature
D	nozzle diameter	$\overline{v}$	velocity vector
H	pedestal height	x_k	coordinate direction
k	turbulent kinetic energy	y	normal distance from wall
L	distance between nozzle and pedestal top surface	δ_{ij}	Kronecker delta
		ε	dissipation rate
p	pressure	∇	gradient/divergence
P_k	production of turbulent kinetic energy	μ	molecular viscosity
Pr	Prandtl number	μ_t	turbulent viscosity
$\overline{q}$	heat flux vector	ρ	density
R_y	dimensionless distance from solid boundary $(=\frac{\rho k^{1/2} y}{\mu})$	$\overline{\overline{\tau}}$	stress tensor
		τ_t	turbulent time scale
$\overline{\overline{S}}$	strain rate tensor	η	dimensionless strain rate $(=\tau_t(S^2+\Omega^2)^{1/2})$
S	strain rate $(=(2S_{ij}S_{ij})^{1/2})$	$\overline{\overline{\Omega}}$	vorticity tensor
S_k	source term for k	Ω	vorticity $(=(2\Omega_{ij}\,\Omega_{ij})^{1/2})$
S_ε	source term for ε		

and Launder (1972), a 'realizable' k–ε model by Shih et al. (1995) and the SST model by Menter (1994), do not provide accurate results. The first-order model of Merci et al. (2004), on the contrary, is reliable.

It is noteworthy that the v^2-f turbulence model by Durbin (1991) has already proved to provide accurate results for impingement heat transfer (Behnia et al., 1998, 1999). However, this is at the cost of two additional equations (a transport equation for v^2 and an elliptic equation for f). For this reason, the presented k–ε model is deemed more suitable, since a comparable level of accuracy is obtained with less computational effort.

In the next section, the experimental set-up and procedure are described. Next, the numerical description is given: the governing equations are listed, the turbulence model is shortly described and the numerical aspects of the simulations are discussed. Finally, the quality of the simulation results is examined through comparison to the experimental data.

2. Experimental set-up and procedure

2.1. Experimental method

The measurement technique is the preheated wall transient method. In this method, a preheated wall is suddenly exposed to an impinging jet. The local heat transfer coefficients are determined from the response of the surface temperature of the wall, exposed to a fluid flow at a different temperature than the initial wall temperature. To that purpose, the color response of liquid crystal on the surface is recorded on video. Liquid crystals are very suitable because their response is repeatable. They are calibrated to establish the relationship between temperature and color transition, which is easily examined with the video system.

Different techniques have been used to accomplish the fluid temperature difference, relative to the surface. In the present study the pedestal mounted surface is heated in a uniform constant temperature oven where temperature control is achieved by a constant temperature calibration bath. Each test piece is then suddenly exposed to an ambient temperature impinging jet by removing an insulating cover. One of the advantages of this technique is that the test piece can have an arbitrary shape.

To measure the surface temperature as the surface is either cooling down or heating up, a fast response type (small time constant) temperature sensor is required. The current study uses microencapsulated thermochromic liquid crystals as surface temperature sensor. Microencapsulated liquid crystals have a very fast response to surface temperature change with a time constant of approximately 10–30 ms, as discussed by Moffat and Anderson (1990). The advantage of using liquid crystals is that it generates a continuous map of the surface response to the temperature change throughout the test run. In addition to visualization for heat transfer process the color change of the liquid crystal can provide some flow visualization.

The current study, which uses the preheated wall transient method, assumes that the heat conduction during the transient process is limited to a very thin layer near the surface. This assumption is generally valid when the material used has a low thermal diffusivity such as Plexiglas (Yan, 1993) which is the material used

for this study. In addition, materials with small penetration depth have been shown to have negligible lateral conduction (Dunne, 1984; Vedula et al., 1988). A simple one-dimensional mathematical model for the transient heat conduction analysis can be used when the above assumptions are valid. The complete mathematical model is found in Mesbah (1996).

Local heat transfer measurements are made along the radial direction for the pedestal top surface and the plate, as well as for the pedestal side surface. The data reduction, providing the local heat transfer coefficient, is described by Ireland and Jones (1985, 1986) and Ireland (1987).

2.2. Apparatus

As mentioned, the preheated wall transient method requires the test piece to be preheated to a constant and uniform temperature prior to measurements. Yan (1993), demonstrated that he achieved a constant and uniform temperature for his experiments using a specially designed oven. Therefore, the same oven is used here for preheating the pedestal surface test piece. A diagram of the heating system used for the pedestal surface test piece including the oven is shown in Fig. 1. The oven consists of a rectangular box made from plywood with Styrofoam insulation (thickness = 0.116 m) on all surfaces. The removable cover provides a completely sealed environment during the heating process.

The oven is heated by hot water which is obtained from a Model 910AC Rosemount constant temperature bath. The water from the constant temperature bath is circulated through a fin type compact heat exchanger

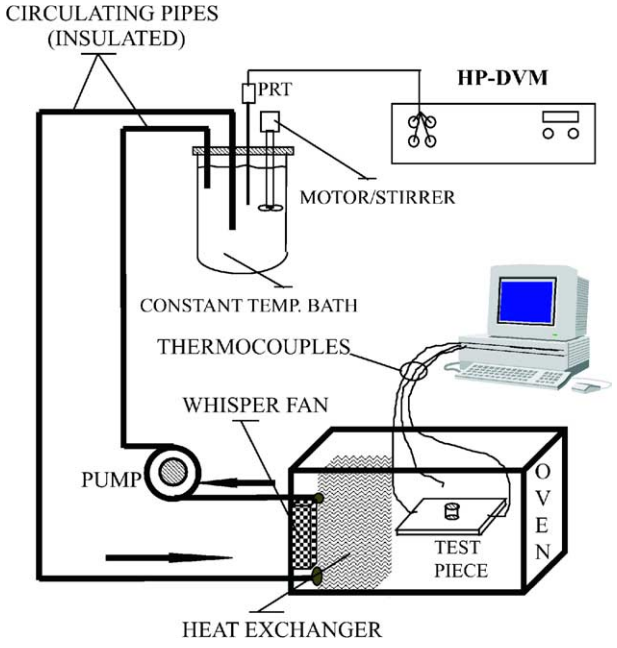

Fig. 1. Heating system for the test piece.

(heater core of a 1966 Ford Mustang) located inside the oven. The initial temperature is set to 48.6 °C. Two thermocouples, measuring the test piece temperature, must agree within 0.1 °C before an experiment is conducted.

The video system used for this study is similar to the system used by Yan (1993). For a typical run, the video image of the liquid crystal color transition from green to red (yellow) with the added time signal is recorded on a VHS tape. The tape is then played back and for each location of interest the heat transfer coefficient can be calculated as mentioned above.

The impinging jet apparatus that is used for the experiments is similar to the apparatus used by Baughn and Shimizu (1989), Baughn et al. (1991), Yan (1993) and Mesbah (1996). The jet emerges from a thin-wall PVC pipe with an inside diameter of 4.03 cm and a length of 64 diameters. The PVC pipe is connected to a 12.7 cm diameter flexible ducting (standard 5 inch diameter aluminum ducting) with an approximate length of 3 m that is also connected to a high power blower. The long section of the flexible ducting, placed at the exit of a room air conditioner, provides for the jet temperature to be maintained the same as the ambient temperature. The velocity distribution just inside the pipe exit is that of a fully-developed pipe flow.

The apparatus is shown in Fig. 2. The test piece consists of a Plexiglas cylindrical pedestal (3.81 cm diameter and 3.81 cm high, giving $D/d = 1.06$, and $H/d = 1$) mounted on a 0.348 m × 0.522 m × 0.006 m thick Plexiglas flat plate with the back side insulated with Styrofoam sheet. The pedestal surface test piece is air brushed with black paint first and then with microincapsulated liquid crystals. A box cover, also made from Styrofoam sheet, provides insulation for the test piece as it is transported from the oven to the test position.

In addition to the actual test piece a dummy test piece of the same dimensions as the actual test piece is prepared. A grid system is attached to the top and the side surfaces of the pedestal and also the extended plate region. This grid system is traced on a transparent plastic sheet and attached on the video monitor screen in order to provide the location of each isotherm as the surface responds to the impinging jet cooling (Mesbah, 1996).

2.3. Procedure

The procedure begins by adjusting the height of the impinging jet for the appropriate L/D (distance to pedestal top surface) while preheating the cylindrical pedestal test piece for 8–10 h in the convection oven until it is at uniform temperature (48.6 ± 0.15 °C) above ambient temperature. After confirming the uniformity of the temperature, the initial temperature is recorded, the dummy test piece is put in place and the image acquisition system is made ready for recording. Using the video

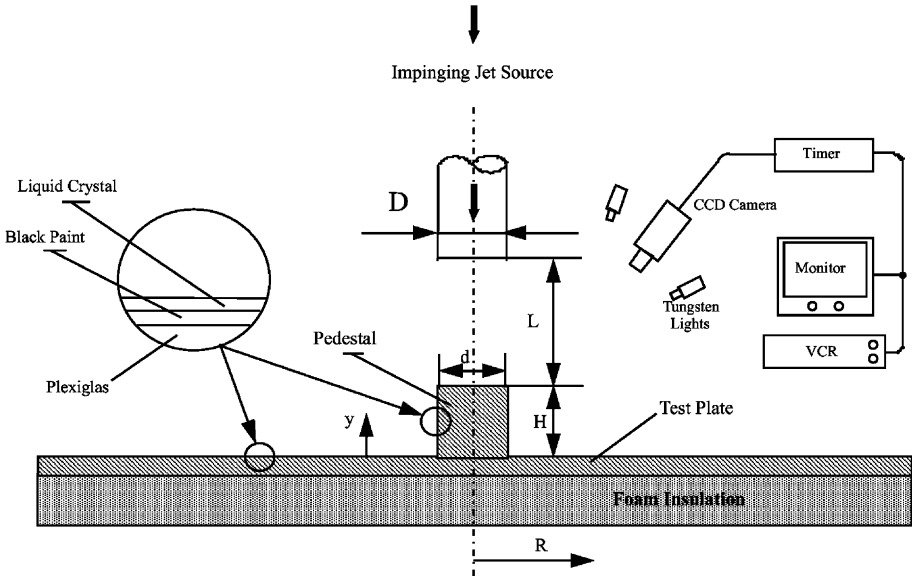

Fig. 2. Impinging jet—pedestal experimental apparatus (not to scale).

type writer, the pertinent header information for each run is recorded on the video tape. The camera is then focused on the entire grid system, the grid system is recorded and the camera is secured in place for the actual test run. The blower is turned on and the flow is adjusted to the required Reynolds number. When the flow is steady, the jet temperature is recorded and then the cylindrical pedestal test piece is removed from the oven with Styrofoam insulation (also preheated in the oven) as it is put into position. With the video system on, the Styrofoam insulation is suddenly removed and the response of the liquid crystal on the surface is recorded.

2.4. Data reduction and uncertainty analysis

A detailed uncertainty analysis is given in Mesbah (1996), including tables of the raw data, using the methods of Coleman and Steele (1999). The uncertainties are estimated as 6% for the heat transfer coefficient and 2% for the Reynolds number.

3. Numerical description

3.1. Governing equations

The averaged steady-state transport equations are

$$\begin{cases} \nabla\cdot(\rho\overline{v}) = 0, \\ \nabla\cdot(\rho\overline{v}\,\overline{v}) + \nabla p = \nabla\cdot(2\mu\overline{\overline{S}} + \overline{\overline{\tau}}'), \\ \nabla\cdot(\rho T\overline{v}) = \nabla\cdot(\overline{q}/c_p), \\ \nabla\cdot(\rho k\overline{v}) = \nabla\cdot[(\mu + \frac{\mu_t}{\sigma_k})(\nabla k)] + S_k, \\ \nabla\cdot(\rho\varepsilon\overline{v}) = \nabla\cdot[(\mu + \frac{\mu_t}{\sigma_\varepsilon})(\nabla\varepsilon)] + S_\varepsilon. \end{cases} \quad (1)$$

Since the density is variable, Favre averaging is used. It is assumed that there are no external forces nor internal heat sources. The strain rate tensor components are:

$$S_{ij} = \frac{1}{2}\left(\frac{\partial v_i}{\partial x_j} + \frac{\partial v_j}{\partial x_i}\right) - \frac{1}{3}\delta_{ij}\frac{\partial v_k}{\partial x_k}. \quad (2)$$

In the energy equation, the contribution of mean and turbulent kinetic energy is neglected and a constant specific heat is assumed. As in Behnia et al. (1998), Behnia et al. (1999) and Craft et al. (2000), the work done by the stress tensor is neglected, too, which is justified by Merci et al. (2003). Consequently, the equation for total enthalpy is formulated in terms of temperature.

The heat flux $\overline{q}$ consists of a molecular and a turbulent part:

$$\overline{q} = -\frac{\mu c_p}{Pr}\nabla T - \frac{\mu_t c_p}{Pr_t}\nabla T, \quad (3)$$

where the linear gradient hypothesis is used for the turbulent heat flux. As was shown by Behnia et al. (1998), a variable turbulent Prandtl number does not significantly affect the results. Therefore, a constant turbulent Prandtl number is used ($Pr_t = 0.9$).

3.2. Turbulence model description

Only the most relevant model features are mentioned here. A complete model description is found elsewhere (Merci and Dick, 2002; Merci and Dick, 2003; Merci et al., 2004). In those references, it is illustrated that the turbulence model yields accurate results for a wide range of flows, without test case dependent parameter tuning.

In Merci et al. (2004), it is illustrated that higher order terms in the expression for the turbulent stresses,

do not influence heat transfer predictions in impingement flow situations noticeably. Therefore, the turbulent stress tensor in (1) is modelled by the first-order expression:

$$\tau_{ij}^{t} = -\rho\overline{v_i' v_j'} = -\frac{2}{3}\rho k\delta_{ij} + 2\mu_t S_{ij}, \tag{4}$$

where μ_t is the eddy viscosity

$$\mu_t = \rho c_{\mu,\mathrm{eff}} k \tau_t \tag{5}$$

with the turbulent time scale

$$\tau_t = \frac{k}{\varepsilon} + \sqrt{\frac{\mu}{\rho\varepsilon}}. \tag{6}$$

The second term in (6) is added because the turbulence model transport equations in Eq. (1) are in low-Reynolds formulation. Thus, singularities are avoided in the calculations up to a solid boundary (e.g. in source term (13)).

The main feature is that $c_{\mu,\mathrm{eff}}$ depends on the local flow field and turbulence quantities. The factor accounts for the effect of streamline curvature and rotation on turbulence. It depends on the dimensionless combination of invariants

$$S = \sqrt{2S_{ij}S_{ij}}, \quad \Omega = \sqrt{2\Omega_{ij}\Omega_{ij}}, \quad \eta = \tau_t(S^2+\Omega^2)^{1/2} \tag{7}$$

with Ω_{ij} the vorticity tensor components

$$\Omega_{ij} = \frac{1}{2}\left(\frac{\partial v_i}{\partial x_j} - \frac{\partial v_j}{\partial x_i}\right). \tag{8}$$

The expression for $c_{\mu,\mathrm{eff}}$ is as in Merci and Dick (2003)

$$\begin{aligned} c_{\mu,\mathrm{eff}} &= c_\mu - \frac{1}{4}c_1\tau_t^2(S^2-\Omega^2) \\ &= \frac{f_\mu}{A_1 + A_s\eta + 25(1-f_{R_y})\,|W|} - \frac{1}{4}c_1\tau_t^2(S^2-\Omega^2) \end{aligned} \tag{9}$$

with $A_1 = 4$, $A_s = \sqrt{3}\cos\phi$ and $\phi = \frac{1}{3}\arccos(\sqrt{6}W)$, with

$$W = 2^{1.5}\frac{S_{ij}S_{jk}S_{ki}}{S^3}. \tag{10}$$

The term with W in (9) prevents excessive levels of turbulent kinetic energy in stagnation regions through a reduction of c_μ in (9) and thus seriously improves stagnation heat transfer predictions. The coefficient c_1 is defined as

$$\begin{cases} S \geqslant \Omega : c_1 = -f_W \min(40c_\mu^4; 0.15), \\ S < \Omega : c_1 = -f_W \min[\min(600c_\mu^4; 0.15), \\ \quad 4f_\mu c_\mu/(\Omega^2\tau_t^2 - S^2\tau_t^2)]. \end{cases} \tag{11}$$

The introduction of f_W improves heat transfer results in stagnation regions

$$f_W = 1 - 18W^2 + (72/\sqrt{6})\,|W|^3. \tag{12}$$

This function turns off the destabilising streamline curvature effect in axisymmetric stagnation regions (where $|W| = 1/\sqrt{6}$). The damping function f_μ is introduced into expression (9) to allow for calculations up to solid boundaries (low-Reynolds formulation).

It is important that accurate values for k and ε are introduced into (4). In this light, the importance of the ε transport equation is well recognized. As explained by Merci and Dick (2003), the proposed source term S_ε in (1) is a combination of the one by Merci et al. (2001) and the one by Shih et al. (1995), with a low-Reynolds source term and a length scale correction

$$S_\varepsilon = (1-f_{R_y})c_{\varepsilon 1}\frac{P_k}{\tau_t} + f_{R_y}C_1 S\rho\varepsilon - c_{\varepsilon 2}f_2\frac{\rho\varepsilon}{\tau_t} + E + Y_c. \tag{13}$$

The blending function f_{R_y} is defined as

$$f_{R_y} = \frac{1}{2} + \frac{1}{2}\sin\left(\frac{\pi}{2}\min[\max(R_y/500 - 3; -1); 1]\right) \tag{14}$$

with $R_y = \frac{\rho\sqrt{k}y}{\mu}$, y being the normal distance from the nearest solid boundary. The blending function goes from 0 to 1 in the interval $R_y = 1000$ to $R_y = 2000$. P_k the production term for turbulent kinetic energy. The parameter C_1 is

$$C_1 = \max\left(0.43; \frac{\eta}{5+\eta}\right). \tag{15}$$

The parameter $c_{\varepsilon 2}$ is

$$c_{\varepsilon 2} = \max\left(1.83 + \frac{0.075\tau_t\Omega}{1+\tau_t^2 S^2}, \quad C_2 f_{R_y}\right) \tag{16}$$

with $C_2 = 1.9$. The damping function is, as suggested by Hanjalic and Launder (1976), $f_2 = 1 - 0.22\exp(-Re_t^2/36)$, with $Re_t = \rho k\tau_t/\mu$ the turbulent Reynolds number. The model constants are $c_{\varepsilon 1} = 1.44$ and $\sigma_\varepsilon = 1.2$. The low-Reynolds source term is

$$E = -1.8(1-f_\mu)\left(\mu + \frac{\mu_t}{\sigma_\varepsilon}\right)\frac{\partial k}{\partial x_i}\frac{\partial \tau_t^{-1}}{\partial x_i}. \tag{17}$$

The final term is a length scale correction, based on Yap (1987), and is the most influential difference from the standard k–ε model with respect to turbulent impingement heat transfer predictions. All other aspects make the model suitable for a wide variety of flows (Merci and Dick, 2002), which are not the topic of this paper. The length scale term is inspired on a suggestion of Craft et al. (2000)

$$\begin{cases} S \leqslant 1.05\Omega : Y_c = 0 \\ S > 1.05\Omega : Y_c = 0.13(1-f_{R_y})\frac{k^2}{y^2}\max\left[\left(\frac{0.4k^{3/2}}{\varepsilon y} - 1\right); 0\right]. \end{cases} \tag{18}$$

It counteracts overprediction of turbulent kinetic energy. It is only added here when streamline curvature has a destabilising effect on turbulence ($S > \Omega$, with a factor 1.05 to avoid numerical problems by alternatingly switching on and off Y_c in regions where $S \approx \Omega$).

The transport equation for k is standard, with $S_k = P_k - \rho\varepsilon$.

3.3. Numerical aspects

Eqs. (1) are solved with the commercial finite volume code FLUENT 6.0. Second-order upwinding is applied to the convective fluxes in the momentum, energy and turbulence equations. For the viscous fluxes, central discretization is applied. Coupling between pressure and velocity is established through the SIMPLE algorithm. The equations are solved in a sequential, rather than in a coupled, manner. Negative parts of the source terms in the turbulence transport equations are treated implicitly. This is in contrast to the method suggested by Merci et al. (2000), but it is sufficient to maintain numerical stability.

The position $x = 0$ corresponding to the nozzle exit, the computational domain (Fig. 3, left) extends from $x = -D/2$ to $x = L + H$, with $D = 1.06H$ the inner nozzle diameter. The domain also ranges from $r = 0$ to $r = 10D$. It consists of 257×125 grid points. In the x-direction, there are 32 cells in the nozzle, 144 cells between $x = 0$ and $x = L$ (i.e. the pedestal top surface) and 80 cells over the pedestal height. The cell distribution is such that the smallest cells are obtained at the pedestal top surface and at the plate (y^+ (or rather x^+) ≈ 1). In the r-direction, there are 80 cells inside the nozzle: 69 cells in $0 < r < H/2$ and 11 in $H/2 < r < D/2$. The smallest cells are square, at the axis and at the side of the pedestal. There is radial stretching towards the outer diameter of the domain.

At the inlet boundary, a (separately calculated) fully developed turbulent pipe flow is imposed in the nozzle, with temperature $T_0 = 295.2\,\mathrm{K}$, as in the experiment ('velocity inlet'). Air entrainment of air around the nozzle is described using a 'pressure inlet' boundary condition, with atmospheric static pressure, temperature $T_0 = 295.2\,\mathrm{K}$, a turbulent intensity of 1% and a turbulent length scale equal to the nozzle diameter. Note that the inlet boundary is upstream of the nozzle exit, so that air entrainment is accurately reproduced.

In the experiments, the plate and pedestal are heated to a uniform temperature (321.2 K) and then cooled by the impinging jet. In this well-known transient method, the amount of cooling is minimized and the thermal boundary condition approaches that of a uniform surface temperature. The heat transfer coefficient is computed from temperature variations in time. In the (steady) calculations, the uniform temperature 321.2 K is imposed on the pedestal and the flat plate and the Nusselt number is computed from the local steady surface heat flux. Velocity components and turbulent kinetic energy are set to zero at the solid boundaries and a zero derivative is used for the static pressure. The dissipation rate is determined as $\varepsilon_w = 2\frac{\mu}{\rho}\left(\frac{\partial\sqrt{k}}{\partial n}\right)^2$, with n the normal to the (solid) boundary.

At the axis, symmetry boundary conditions are used. At the upper boundary, atmospheric static pressure is imposed and radial derivatives for the other quantities are set to zero ('pressure outlet' condition).

All the presented results have been checked with respect to grid independence: the grid has been refined in both directions and variations of variables in monitoring points are less than 0.5%.

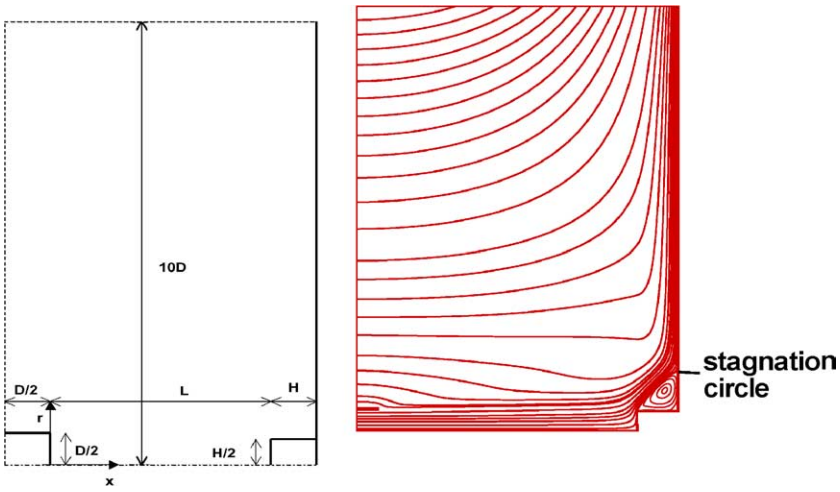

Fig. 3. (left) Geometry and computational domain and (right) streamline pattern.

4. Results and discussion

Results are presented for different turbulence models. The standard k–ε model by Jones and Launder (1972), in high-Reynolds formulation, is combined with the one-equation model of Wolfstein (1969) in the neighbourhood of solid boundaries (which is defined here by the criterion $R_y = \rho\sqrt{k}y/\mu < 200$). In this one-equation model, the transport equation for k is standard, but the eddy viscosity is defined as by Chen and Patel (1988): $\mu_{t,visc} = \rho c_\mu l_\mu \sqrt{k}$, with $c_\mu = 0.09$ and $l_\mu = \kappa c_\mu^{-3/4} y(1 - \exp(-R_y/70))$, with $\kappa = 0.4$ the von Karman constant. The dissipation rate is determined from $\varepsilon = k^{3/2}/l_\varepsilon$, with l_ε defined in a similar manner as l_μ (Chen and Patel, 1988). In the 'turbulent' region, the standard k–ε model by Jones and Launder (1972) is used, with the eddy viscosity $\mu_t = \rho c_\mu k^2/\varepsilon$. In the complete flow domain, a blending is applied: $\mu_{t,eff} = \alpha\mu_t + (1-\alpha)\mu_{t,visc}$, where the blending factor $\alpha = \frac{1}{2}\left(1 + \tanh\left(\frac{R_y - 200}{30}\right)\right)$ is zero at the wall and goes to one when R_y becomes sufficiently large. The combination with the one-equation model is denoted as 'e.w.t.' in the figures, which stands for 'enhanced wall treatment'.

Beside this 'two-layer' model, the high-Reynolds SST model by Menter (1994) is applied. It is noted that no special action has been taken to improve stagnation point heat transfer predictions through limitations of the turbulent length scale or production term. Also the 'realizable' k–ε model of Shih et al. (1995) is tested. This model is combined with the same one-equation model as described above. Finally, results are also presented with the model described above. Since this model is in low-Reynolds formulation, no combination with the one-equation model is necessary.

In Fig. 3 (right), a typical streamline pattern is shown. At the nozzle exit, air entrainment is observed. Around the pedestal, an axisymmetric recirculation region exists. At the pedestal's top face, a stagnating streamline is positioned on the symmetry axis. Around the recirculation region, a second stagnation point is observed, which is pointed as 'stagnation circle'.

In Fig. 4, isolines of turbulent kinetic energy are presented. The maximum value is near the pedestal top corner, due to the large turbulent shear stresses in the curved streamlines in that regions. Also high levels of turbulent kinetic energy are predicted on the symmetry axis and near the stagnation circle. Unfortunately, there are no experimental data to confirm this pattern of turbulent kinetic energy. Indirect confirmation is obtained through the surface heat transfer coefficient profiles, though, as is discussed next. It is noteworthy that the iso-levels are higher with the SST model than with the k–ε (e.w.t.) and the present model, while the patterns are very similar.

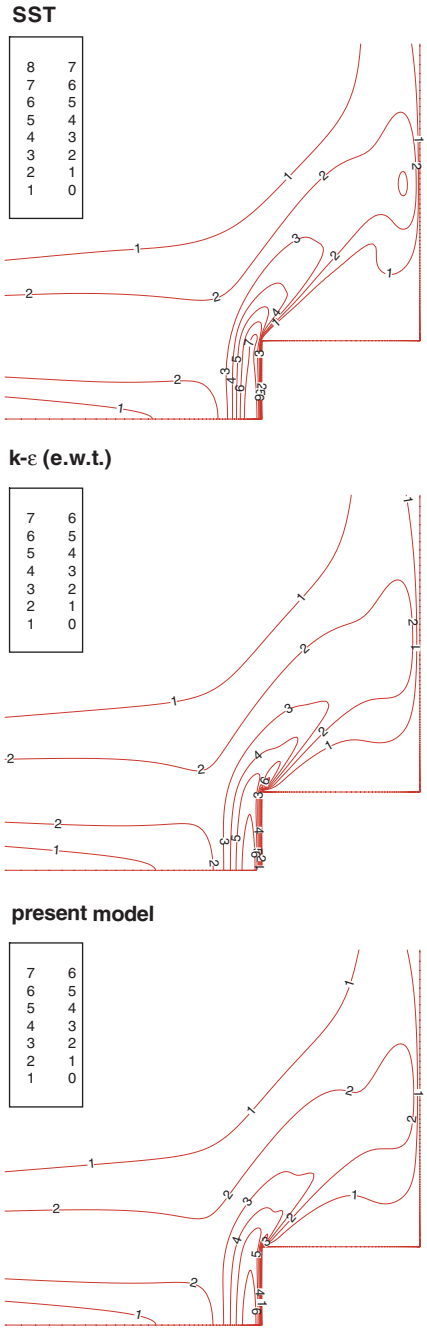

Fig. 4. Field patterns of turbulent kinetic energy (in m^2/s^2).

Fig. 5 presents profiles for the surface heat transfer coefficient along the pedestal's top face (left) and the plate (right), for a nozzle–pedestal distance equal to $L = 6D$, for different Reynolds numbers. The discussion is firstly restricted to $Re = 23{,}000$, based on jet bulk velocity and nozzle diameter. Afterwards, the Reynolds dependence is discussed.

As mentioned by Behnia et al. (1999), the experiments show a local minimum in the heat transfer coefficient on the symmetry axis, which is in contrast to observations on a simple flat plate. Fig. 4 provides the explanation:

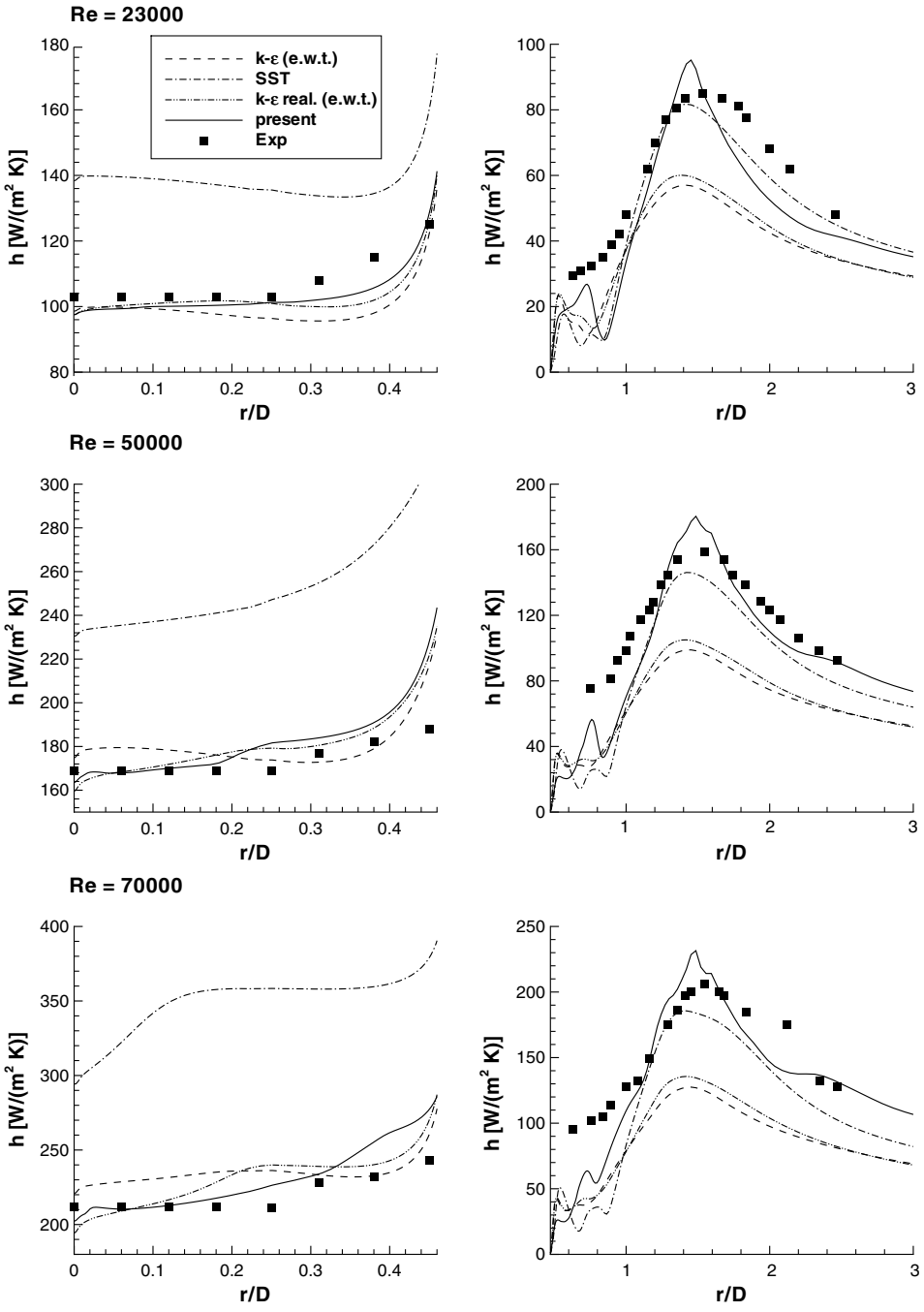

Fig. 5. Surface heat transfer coefficient at the pedestal's top face and along the flat plate for different Reynolds numbers.

the maximum level of turbulent kinetic energy appears to be near the pedestal corner, resulting in an increased local heat transfer. The present model is the only one of the models under study which correctly reproduces this qualitative behaviour. The SST model and the standard k–ε (e.w.t.) model predict the minimum at $r \approx 0.35D$. With the realizable k–ε (e.w.t.) model, this minimum is less pronounced, but the trend is still visible. It is noteworthy that the $v^2 - f$ model by Durbin (1991) reproduces the qualitative behaviour correctly, too, as shown by Behnia et al. (1999).

The good agreement of the stagnation heat transfer coefficient with the standard and the realizable k–ε model, are due to the combination with the one-equation turbulence model. Its main effect is indeed that the eddy viscosity in stagnating flow regions is strongly reduced in comparison with the high-Reynolds number formulation. Consequently, the classical overprediction of impingement heat transfer is avoided. The low-Reynolds formulation of Yang and Shih (1993) does not cure the heat transfer overprediction, as illustrated by Merci and Dick (2003), because the damping function only be-

comes effective when $R_y < 100$, while the peak in turbulent kinetic energy is positioned at larger values of R_y, which are indeed affected with the two-layer approach. The good agreement with the present model is mainly due to the length scale term (18) and the expression for $c_{\mu,\text{eff}}$ (9). With the SST model, heat transfer is strongly over-predicted. This is in accordance with the higher level of turbulent kinetic energy with this model, as already mentioned (Fig. 4).

Around the pedestal, however, the advantage of the 'enhanced wall treatment' on the pedestal's top face, becomes a disadvantage. Indeed, the surface heat transfer coefficient is strongly underestimated with the standard and realizable k–ε models with e.w.t. (Fig. 5, right). With the SST model, better agreement is obtained, but at the cost of worse predictions on the pedestal's top face. With the present model, agreement is acceptable along the plate. Again, it should be noted that a comparable level of accuracy is shown with the $v^2 - f$ model by Behnia et al. (1999).

The radial distribution of the local heat transfer coefficient does not vary over the studied range of L/D ratios (i.e. $L/D = 1$ to $L/D = 6$). This is in contrast to what is observed for a flat plate. The reason is that the flow structure, in particular around the pedestal, is independent of the fact whether the jet is fully developed or not: there is a recirculation region around the pedestal and a stagnation circle around the pedestal. The latter causes the peak in the local heat transfer coefficient at around $r = 1.5D$. The shape on the pedestal's side face remains unaltered for the same reason: the recirculation region around the pedestal exists, regardless of the L/D ratio. On the pedestal top face, the shape remains unaltered, too, but this may be due to the fact that the pedestal diameter is not sufficiently large, compared to the jet diameter. If the latter were the case, the influence of the jet being fully developed or not before hitting the pedestal, may well be visible on the pedestal top face. Since the radial distribution remains unchanged regardless of the L/D ratio for the test case under study, results are shown only for $L/D = 6$.

At the intersection of the pedestal with the plate ($r \approx D/2$), the heat transfer coefficient is strongly underpredicted by all models. This is due to the steadiness of the simulations. The air is trapped in the recirculation region, while in reality there is unsteadiness and 'fresh' air can reach the pedestal's bottom corner. Consequently, the mean heat transfer increases. Such features cannot be captured with steady simulations. A similar underprediction is reported with the $v^2 - f$ model by Behnia et al. (1999).

With respect to Reynolds number dependence of the results, it is observed in Fig. 5 that the above findings remain valid for all models at higher Reynolds numbers. The profiles with the present model are slightly less smooth, but the global quality remains acceptable and better than for all considered standard models. In particular the stagnation point values are well predicted, both on the pedestal and the plate.

Fig. 6 shows the local heat transfer coefficients along the pedestal side face. The peak in the local heat transfer is near the bottom corner of the pedestal. Indeed, there is some kind of soft impingement of the flow in the recirculation region onto the pedestal side face in that region. It is observed that all models are comparable in quality. All predict the shape correctly, but the absolute values are too low, compared to the experimental observations. This statement holds for all considered Reynolds numbers.

Fig. 7 (left) shows the dependence of the stagnation heat transfer coefficient on the Reynolds number for a fixed nozzle–pedestal distance $L = 6D$. Clearly, the slope of the lines in the log–log diagram is in acceptable agreement with the experiments for all models, except perhaps for the standard k–ε (e.w.t.) model, which shows a slightly steeper behaviour. Table 1 summarizes the exponent n in the relation $h \sim Re^n$ for the different models.

The right-hand side of Fig. 7 presents the influence on the stagnation heat transfer of the distance between the nozzle and the pedestal top surface for $Re = 23{,}000$. Globally, the present model has the best qualitative

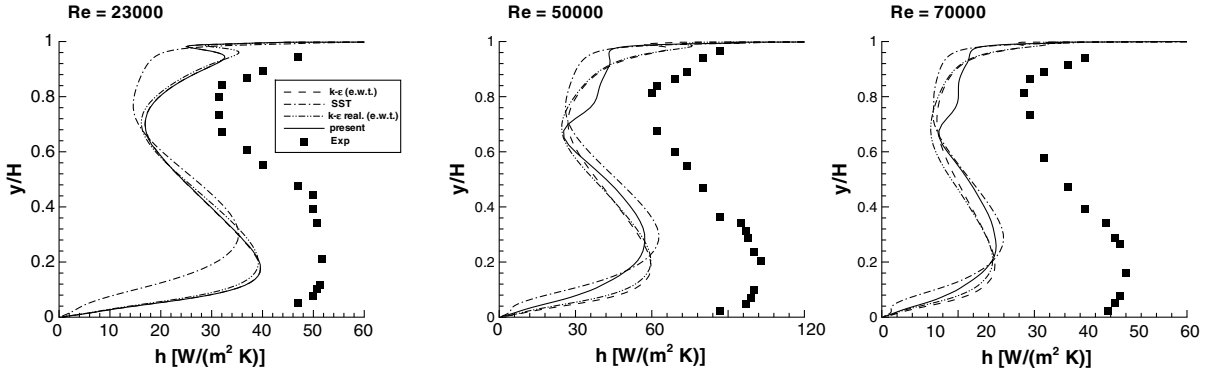

Fig. 6. Surface heat transfer coefficient at the pedestal's side face for different Reynolds numbers.

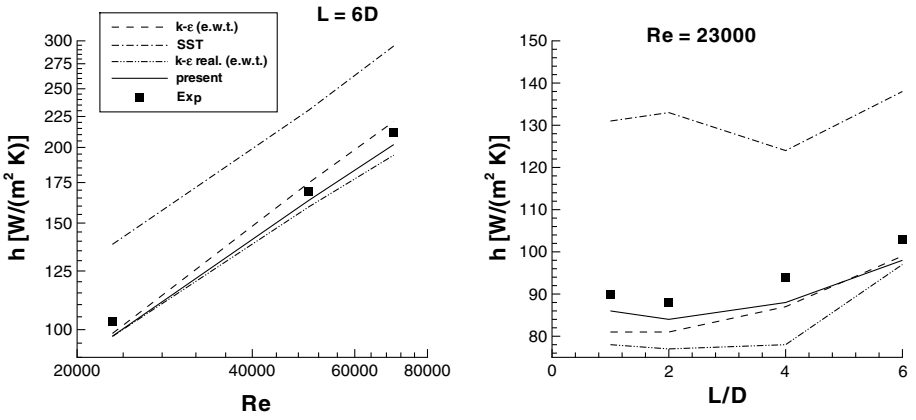

Fig. 7. Dependence of stagnation point surface heat transfer coefficient on Reynolds number (left) and on distance between nozzle and pedestal (right).

Table 1
Value of exponent n in relation $h \sim Re^n$

Model	k–ε (e.w.t.)	SST	Real. k–ε (e.w.t.)	Present	Exp.
n	0.72	0.68	0.62	0.65	0.64

agreement with the experimental data. The SST model predicts a pronounced minimum for $L = 4D$ (while the experiments indicate a minimum for $L = 2D$). The realizable k–ε (e.w.t.) model reveals too strong variations between $L = 4D$ and $L = 6D$. The standard k–ε (e.w.t.) model does not reproduce the higher heat transfer for $L = D$ (compared to $L = 2D$).

5. Conclusions

An experimental and numerical study has been presented of the local turbulent heat transfer of a round jet, impinging onto a pedestal, mounted on a flat plate. Only one configuration has been studied in detail in the present work. Experimental data for other nozzle–pedestal distances are found in Mesbah (1996). An advanced new k–ε model has been applied to this complex test case.

The global quality of the presented two-equation turbulence model has been illustrated. The local heat transfer coefficient on both the pedestal top surface and the plate are correctly reproduced, in contrast to what is obtained with standard models. This has been demonstrated for three different Reynolds numbers. On the pedestal side surface, the quality of the turbulence model is comparable to that of the standard models. The shape of the heat transfer coefficient profile is correct, but the absolute values are underestimated.

The influence on the stagnation point heat transfer of variations of the Reynolds number with a fixed nozzle–pedestal distance, as well as different nozzle–pedestal distances with a fixed Reynolds number, has been investigated. The present model performs well for all cases without any parameter tuning, in contrast to the considered standard turbulence models.

Acknowledgment

The first author is a Postdoctoral Fellow of the Fund for Scientific Research-Flanders (Belgium) (F.W.O.-Vlaanderen).

References

Baughn, J.W., Shimizu, S., 1989. Heat transfer measurements from a surface with uniform heat flux and an impinging jet. J. Heat Transfer 111, 1096–1098.

Baughn, J.W., Hechanova, A., Yan, X., 1991. An experimental study of entrainment effects on the heat transfer from a flat surface to a heated circular impinging jet. J. Heat Transfer 113 (4), 1023–1025.

Behnia, M., Parneix, S., Durbin, P.A., 1998. Prediction of heat transfer in an axisymmetric turbulent jet impinging on a flat plate. Int. J. Heat Mass Transfer 41 (12), 1845–1855.

Behnia, M., Parneix, S., Shabany, Y., Durbin, P.A., 1999. Numerical study of turbulent heat transfer in confined and unconfined impinging jets. Int. J. Heat Fluid Flow 20, 1–9.

Chen, H.C., Patel, V.C., 1988. Near-wall turbulence models for complex flows including separation. AIAA J. 26 (6), 641–648.

Coleman, H.W., Steele, W.G., 1999. Experimentation and Uncertainty Analysis for Engineers, second ed. John Wiley, New York.

Craft, T.J., Iacovides, H., Yoon, J.H., 2000. Progress in the use of non-linear two-equation models in the computation of convective heat-transfer in impinging and separated flows. Flow, Turbul. Combust. 63, 59–80.

Dunne, S.T., 1984. A study of flow and heat transfer in gas turbine cooling passages. D.Phil. Thesis, Oxford University, Oxford, UK.

Durbin, P., 1991. Near-wall turbulence closure without damping functions. Theor. Comp. Fluid Dyn. 3, 1–13.

Hanjalic, K., Launder, B.E., 1976. Contribution towards a Reynolds-stress closure for low-Reynolds-number turbulence. J. Fluid Mech. 74 (4), 593–610.

Ireland, P.T., 1987. Internal cooling of turbine blades. D. Phil. Thesis, Oxford University, Oxford, UK.

Ireland, P.T., Jones, T.V., 1985. The measurement of local heat transfer coefficients in blade cooling geometries. In: AGARD Conference Proceedings No. 390, Paper 28.

Ireland, P.T., Jones, T.V., 1986. Detailed measurements of heat transfer on and around a pedestal in fully developed passage flow. In: Proceedings of the 8th International Heat Transfer Conference, vol. 3, pp. 975–980.

Jones, W.P., Launder, B.E., 1972. The prediction of laminarization with a two-equation model of turbulence. Int. J. Heat Mass Transfer 15 (2), 301–314.

Lytle, D., Webb, B., 1994. Air jet impingement heat transfer at low nozzle–plate spaces. Int. J. Heat Mass Transfer 37 (12), 1687–1697.

Menter, F.R., 1994. Two-equation eddy-viscosity turbulence models for engineering applications. AIAA J. 32 (8), 1598–1605.

Merci, B., Dick, E., 2002. Predictive capabilities of an improved cubic k–ε model for inert steady flows. Flow, Turbulence Combust. 68 (4), 335–358.

Merci, B., Dick, E., 2003. Heat transfer predictions with a cubic k–ε model for axisymmetric turbulent jets impinging onto a flat plate. Int. J. Heat Mass Transfer 46 (3), 469–480.

Merci, B., Steelant, J., Vierendeels, J., Riemslagh, K., Dick, E., 2000. Computational treatment of source terms in two-equation turbulence models. AIAA J. 38 (11), 2085–2093.

Merci, B., De Langhe, C., Vierendeels, J., Dick, E., 2001. A quasi-realizable cubic low-Reynolds eddy-viscosity turbulence model with a new dissipation rate equation. Flow, Turbul. Combust. 66 (2), 133–157.

Merci, B., Vierendeels, J., De Langhe, C., Dick, E., 2003. Numerical simulation of heat transfer of turbulent impinging jets with two-equation turbulence models. Int. J. Numer. Methods Heat Fluid Flow 13 (1), 110–132.

Merci, B., De Langhe, C., Lodefier, K., Dick, E., 2004. Axisymmetric impingement heat transfer with a non-linear k–ε model. J. Thermophys. Heat Transfer 18 (1), 100–107.

Mesbah, M.P.E., 1996. An experimental study of local heat transfer to an impinging jet on non-flat surfaces: a cylindrical pedestal and a hemispherically concave surface. Ph.D. Thesis, University of California, Davis.

Moffat, R.J., Anderson, A.M., 1990. Applying heat-transfer coefficient data to electronics cooling. J. Heat Transfer—T ASME 112 (4), 882–890.

Shih, T.H., Liou, W.W., Shabbir, A., Yang, Z., Zhu, J., 1995. A new k–ε eddy viscosity model for high Reynolds number turbulent flows. Comput. Fluids 24 (3), 227–238.

Vedula, R.P., Metzger, D.E., Bickford, W.B., 1988. Effect of lateral and anisotropic conduction on determination of local convection heat transfer characteristics with transient tests and surface coatings. In: ASME Collected Papers in Heat Transfer, vol. 104, pp. 21–27.

Wolfstein, M., 1969. The velocity and temperature distribution of one-dimensional flow with turbulence augmentation and pressure gradient. Int. J. Heat Mass Transfer 12, 301–318.

Yan, X., 1993. A preheated-wall transient method using liquid crystals for the measurement of heat transfer on external surfaces and in ducts. Ph.D. Thesis, University of California, Davis.

Yang, Z.Y., Shih, T.H., 1993. A new time scale based $k-\epsilon$ model for near-wall turbulence. AIAA J. 31 (7), 1191–1198.

Yap, C.R., 1987. Turbulent heat and momentum transfer in recirculating and impinging flows. Ph.D. Thesis, University of Manchester, UK.